Monthly Notices of the ROYAL ASTRONOMICAL SOCIETY

MNRAS **473,** 3500–3506 (2018) doi:10.1093/mnras/stx2552
Advance Access publication 2017 October 24

On the maximum energy of non-thermal particles in the primary hotspot of Cygnus A

Anabella T. Araudo,[1,2]★ Anthony R. Bell,[3] Katherine M. Blundell[4] and James H. Matthews[4]

[1]*Astronomical Institute of the Czech Academy of Sciences, Bocni II 1401, Prague CZ-14100, Czech Republic*
[2]*Laboratoire Univers et Particules de Montpellier CNRS/Universite de Montpellier, Place E. Bataillon, F-34095 Montpellier, France*
[3]*University of Oxford, Clarendon Laboratory, Parks Road, Oxford OX1 3PU, UK*
[4]*University of Oxford, Astrophysics, Keble Road, Oxford OX1 3RH, UK*

Accepted 2017 September 26. Received 2017 September 26; in original form 2017 May 24

ABSTRACT

We study particle acceleration and magnetic field amplification in the primary hotspot in the north-west jet of radiogalaxy Cygnus A. By using the observed flux density at 43 GHz in a well-resolved region of this hotspot, we determine the minimum value of the jet density and constrain the magnitude of the magnetic field. We find that a jet with density greater than 5×10^{-5} cm^{-3} and hotspot magnetic field in the range 50–400 μG are required to explain the synchrotron emission at 43 GHz. The upper-energy cut-off in the hotspot synchrotron spectrum is at a frequency $\lesssim 5 \times 10^{14}$ Hz, indicating that the maximum energy of non-thermal electrons accelerated at the jet reverse shock is $E_{\rm e,max} \sim 0.8$ TeV in a magnetic field of 100 μG. Based on the condition that the magnetic-turbulence scalelength has to be larger than the plasma skin depth, and that the energy density in non-thermal particles cannot violate the limit imposed by the jet kinetic luminosity, we show that $E_{\rm e,max}$ cannot be constrained by synchrotron losses as traditionally assumed. In addition to that, and assuming that the shock is quasi-perpendicular, we show that non-resonant hybrid instabilities generated by the streaming of cosmic rays with energy $E_{\rm e,max}$ can grow fast enough to amplify the jet magnetic field up to 50–400 μG and accelerate particles up to the maximum energy $E_{\rm e,max}$ observed in the Cygnus A primary hotspot.

Key words: acceleration of particles – radiation mechanisms: non-thermal – shock waves – galaxies: active – galaxies: individual: Cygnus A – galaxies: jets.

1 INTRODUCTION

Type II Fanaroff–Riley (FR) radiogalaxies exhibit well-collimated jets with bright radio synchrotron knots (hotspots) at the termination region. Electrons radiating in the hotspot are locally accelerated in the jet reverse shock, and they reach a maximum energy $E_{\rm e,max}$ inferred from the Infrared (IR)/optical cut-off frequency ($\nu_{\rm c}$) of the synchrotron spectrum:

$$\frac{E_{\rm e,max}}{\rm TeV} \sim 0.8 \left(\frac{\nu_{\rm c}}{5\times10^{14}\,{\rm Hz}}\right)^{\frac{1}{2}} \left(\frac{B}{100\,\mu{\rm G}}\right)^{-\frac{1}{2}}, \quad (1)$$

where B is the magnetic field (e.g. Meisenheimer & Heavens 1986; Brunetti et al. 2003). In some cases, X-rays are also detected and modelled as synchrotron self-Compton emission and Compton up-scattering of cosmic microwave background photons (e.g. Wilson, Young & Shopbell 2000; Perlman et al. 2010). We note however that in very few cases X-ray synchrotron emission is proposed (Tingay et al. 2008; Orienti et al. 2017).

Ions can also be accelerated in the jet reverse shock. Given that hadronic losses are very slow in low density plasmas such as the termination region of FR II radiogalaxy jets, protons might achieve energies as large as the limit imposed by the size of the system, usually called 'Hillas limit' (Lagage & Cesarsky 1983; Hillas 1984). In particular, mildly relativistic shocks with velocity $v_{\rm sh} = c/3$ might accelerate particles with Larmor radius $r_{\rm g} \sim R_{\rm j}$, where $R_{\rm j}$ is the jet width at the termination region. Particles with such a large $r_{\rm g}$ have energy

$$\frac{E_{\rm Hillas}}{\rm EeV} \sim 100 \left(\frac{v_{\rm sh}}{c/3}\right) \left(\frac{B}{100\,\mu{\rm G}}\right) \left(\frac{R_{\rm j}}{\rm kpc}\right), \quad (2)$$

as expected for Ultra High Energy Cosmic Rays (UHECRs) (e.g. Rachen & Biermann 1993; Norman, Melrose & Achterberg 1995). Bell et al. (2017) examine the maximum energy to which Cosmic Rays (CR) can be accelerated by relativistic shocks, showing that acceleration of protons to 100 EeV is unlikely (See also

★ E-mail: anabella.araudo@asu.cas.cz

Kirk & Reville 2010; Lemoine & Pelletier 2010; Sironi, Spitkovsky & Arons 2013; Reville & Bell 2014).

In Araudo et al. (2016), we have shown that hotspots of FR II radiogalaxies are very poor accelerators. We have shown that the maximum energy of non-thermal electrons accelerated at the reverse shocks is not determined by synchrotron losses, unless very extreme conditions in the plasma are assumed[1]. By equating the acceleration and synchrotron cooling time-scales, we show that the mean free path of the most energetic electrons accelerated at the jet termination shocks is greater than the maximum value imposed by plasma physics for canonical values of the magnetic field and jet density. We demonstrated this by considering the sample of eight hotspots observed with high spatial resolution at optical, IR and radio wavelengths by Mack et al. (2009).

If synchrotron losses do not balance energy gain, the electrons' maximum energy $E_{\rm e,max}$ is ultimately determined by the ability to scatter particles in the shock environment, and this limit applies to both electrons and protons. Assuming that the jet magnetic field downstream of the shock is quasi-perpendicular, we found that non-resonant (Bell) turbulence generated by the streaming of CRs can grow fast enough to amplify the jet magnetic field by about two orders of magnitude and accelerate particles up to $E_{\rm e,max} \sim 0.1-1$ TeV.

In this paper, we study the FR II radiogalaxy Cygnus A, having a redshift $z \sim 0.05607$ ($d \sim 227.3$ Mpc, where d is the distance from Earth) in the Cygnus galaxy cluster (Owen et al. 1997). The north-west jet terminates at ∼60 kpc from the central source where the primary (B) and secondary (A) hotspots are detected [2]. Stawarz et al. (2007) modelled the radio-to-X-rays non-thermal emission from the secondary hotspots in the one-zone approximation and assumed that $E_{\rm e,max}$ is determined by synchrotron cooling. In this work, we apply the same methodology presented in Araudo et al. (2016) to the north-west primary hotspot. We improve our previous model by removing the assumption that the jet density (at the termination region) is $n_{\rm jet} = 10^{-4}$ cm^{-3}. Using the 43 GHz high spatial resolution data, we constrain the magnetic field and the jet density (Section 2.1). On the other hand, using the cut-off of the synchrotron spectrum determined from IR and optical emission, we show that $E_{\rm e,max}$ cannot be determined by synchrotron cooling, unless the jet density is of the order of the density in the external medium (Section 3). Finally, assuming that the magnetic field downstream of the shock is quasi-perpendicular, we constrain the scale size of magnetic turbulence (Section 4.1) and show that it can be excited through the non-resonant hybrid (NRH) instability (Section 4.2). We conclude that the primary hotspot in Cygnus A is a clear example where particle acceleration is not constrained by synchrotron losses. Throughout this paper, we use cgs units and the cosmology $H_0 = 71$ km s^{-1} Mpc^{-1}, $\Omega_0 = 1$ and $\Lambda_0 = 0.73$. One arcsecond represents 1.044 kpc on the plane of the sky at $z = 0.05607$.

2 SYNCHROTRON RADIO EMISSION FROM THE NORTH-WEST PRIMARY HOTSPOT

The north-west primary hotspot has been detected with the MERLIN interferometer at 151 MHz (Leahy, Muxlow & Stephens 1989) and with the Very Large Array (VLA) at frequencies from 327 MHz to 87 GHz (e.g. Carilli et al. 1991). In addition to that, 230 GHz emission was detected with the BIMA array with 1 arcsec angular resolution. Wright & Birkinshaw (2004) made spectral index maps and found that the 5–230, 5–15, and 15–230 GHz spectral indices are $\alpha_5^{230} = \alpha_5^{15} = \alpha_{15}^{230} = 1.13$, whereas $\alpha_{87}^{230} = 1.23$. Therefore, no spectral break is observed between 5 and 230 GHz. These steep radio spectral indices would indicate that electrons emitting synchrotron radiation at these frequencies radiate most of their energy in the hotspot. However, recent analysis from the same set of VLA data shows that the spectral index from 5 to 43 GHz is $\alpha_5^{43} \sim 0.72$ (Pyrzas, Steenbrugge & Blundell 2015), consistent with standard diffusive shock acceleration in the slow cooling regime. In the following section, we will consider the well-resolved emission at 43 GHz to constrain the value of the magnetic field[3].

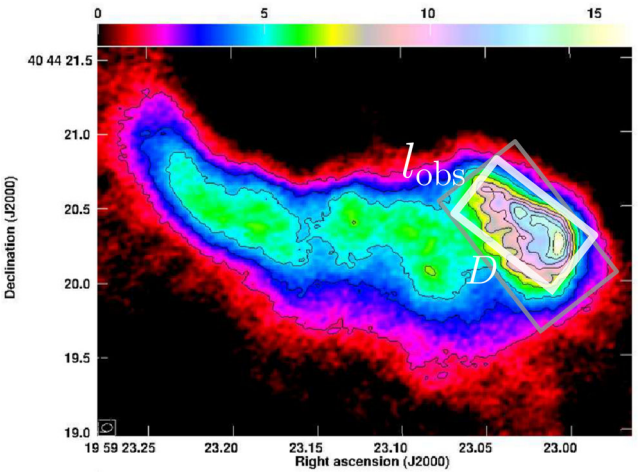

Figure 1. Cygnus A primary hotspot at 43 GHz. The grey rectangle indicates region considered in Pyrzas et al. (2015) to compute the spectral index, whereas the white rectangle of size $l_{\rm obs} = 0.5$ arcsec and $D = 0.9$ arcsec is the region considered in our study to compute the magnetic field in the hotspot. It is approximately drawn to match the half height points of the emission profile. Adapted from Pyrzas et al. (2015).

2.1 Constraining the magnetic field with the synchrotron emission at 43 GHz

Fig. 1 shows the hotspot at 43 GHz, where the region considered by Pyrzas et al. (2015) to calculate the spectral index (α_5^{43}) is indicated by the grey rectangle of 0.7×1.2 arcsec^2. For our study, we select a region of 0.5×0.9 arcsec^2 (indicated by the white rectangle in Fig. 1) defined by the half-height points of the emission peak. Considering that the radio emitter is a cylinder of diameter $D = 0.9$ arcsec and width (projected in the plane of the sky) $l_{\rm obs} = 0.5$ arcsec, the emitter volume at 43 GHz is $V = \pi D^2 l_{\rm obs}/4 \sim 0.32$ arcsec^3 (i.e. $V \sim 0.36$ kpc^3). The background emission corrected flux at 43 GHz is $f_{43} = 0.36$ Jy (Pyrzas et al. 2015), and the specific luminosity is $L_{43} = 43 \times 10^9 f_{43} 4\pi {\rm d}^2 \sim 9 \times 10^{41}$ erg s^{-1}. We model the synchrotron radio emission in V as produced by non-thermal electrons following a power-law energy distribution $N_{\rm e} \propto E_{\rm e}^{-p}$, with $p = 2\alpha_5^{43} + 1 = 2.44$ and $E_{\rm e} \geq E_{\rm e,min} = m_{\rm e}c^2\gamma_{\rm e,min}$, where

$$\gamma_{\rm e,min} \sim 450 \left(\frac{\nu_{\rm min}}{0.1\,{\rm GHz}}\right)^{\frac{1}{2}} \left(\frac{B}{100\,\mu{\rm G}}\right)^{-\frac{1}{2}} \quad (3)$$

[1] In our previous papers, we called $E_{\rm c} = E_{\rm e,max}$ and $E_{\rm uhecr} = E_{\rm Hillas}$.

[2] The north-west primary and secondary hotspots are sometimes called B and A, respectively (e.g. Stawarz et al. 2007).

[3] The VLA beam-size at 43 GHz is 0.07×0.06 arcsec^2.

Table 1. Physical parameters of the north-west primary hotspot.

$z = 0.05607$	$d = 227.3$ Mpc	1arcsec = 1.044 kpc
$\alpha = 0.72$	$p = 2.44$	
$\nu_{\rm min} = 0.1$ GHz	$\nu = 43$ GHz	$\nu_{\rm c} = 5 \times 10^{14}$ Hz
	43 GHz	
$l_{\rm obs} = 0.5$ arcsec	$D = 0.9$ arcsec	$V = 0.36\,{\rm kpc}^3$
$f_{43} = 0.36$ Jy	$L_{43} = 9 \times 10^{41}$ erg s^{-1}	$B_{\rm eq} = 390\,\mu$G ($a = 1$)
$v_{\rm jet}$	$\Gamma_{\rm jet}$	$n_{\rm jet,min}$ [cm^{-3}]
$c/2$	1.15	5.44×10^{-5} ($a = 1$)
$c/3$	1.06	1.36×10^{-4} ($a = 1$)
$c/5$	1.02	4.08×10^{-4} ($a = 1$)

and $\nu_{\rm min}$ is the frequency of the low-energy turnover[4] (e.g. McKean et al. 2016). We insert $\gamma_{\rm e,min}$ and the numerical values of V, p, ν and L_{43} (see Table 1) in equations (20) and (21) in Araudo et al. (2016). We find that the energy density in non-thermal electrons determined from the synchrotron emission at 43 GHz is

$$\frac{U_{\rm e}}{\rm erg\,cm^{-3}} \sim 2\times10^{-8}\left(\frac{\nu_{\rm min}}{0.1\,\rm GHz}\right)^{-0.22}\left(\frac{B}{100\,\mu\rm G}\right)^{-\frac{3}{2}} \times\left(\frac{V}{0.36\,\rm kpc^3}\right)^{-1}, \quad (4)$$

and the magnetic field in equipartition with non-thermal electrons and protons would be

$$\frac{B_{\rm eq}}{\mu\rm G} \sim 390\left(\frac{1+a}{2}\right)^{\frac{2}{7}}\left(\frac{\nu_{\rm min}}{0.1\,\rm GHz}\right)^{-0.06}\left(\frac{V}{0.36\,\rm kpc^3}\right)^{-\frac{2}{7}}, \quad (5)$$

where the energy density in non-thermal protons is $U_{\rm p} = aU_{\rm e}$, and therefore the non-thermal energy density is $U_{\rm nt} = (1+a)U_{\rm e}$. Note the weak dependence of $U_{\rm e}$ and $B_{\rm eq}$ on $\nu_{\rm min}$. We keep V fixed in equations (4) and (5).

The jets of Cygnus A suggest a precession pattern from which the jet velocity was estimated as $0.2 < v_{\rm jet} < 0.5c$ in the termination region (see Steenbrugge & Blundell 2008, and references therein). The jet kinetic energy density is

$$\frac{U_{\rm kin}}{\rm erg\,cm^{-3}} \sim 9\times10^{-9}\left(\frac{n_{\rm jet}}{10^{-4}\,\rm cm^{-3}}\right)\left(\frac{\Gamma_{\rm jet}-1}{0.06}\right), \quad (6)$$

where $\Gamma_{\rm jet} = 1.06$ is the jet bulk Lorentz factor when $v_{\rm jet} = c/3$ (see Table 1). By setting the extreme condition $U_{\rm kin} = 2B_{\rm eq}^2/(8\pi)$, i.e. all the jet kinetic energy density in the shock upstream region is converted into magnetic ($U_{\rm mag}$) and non-thermal ($U_{\rm nt}$) energy densities in the downstream region (the hotspot) and that $U_{\rm mag} = U_{\rm nt} = (1+a)U_{\rm e}$ (the equipartition condition), the minimum jet matter density (at the termination region) is

$$n_{\rm jet,min} = 2\left(\frac{B_{\rm eq}^2}{8\pi}\right)\left(\frac{1}{m_{\rm p}c^2(\Gamma_{\rm jet}-1)}\right) \sim 1.36\times10^{-4}\left(\frac{1+a}{2}\right)^{\frac{4}{7}}\left(\frac{\nu_{\rm min}}{0.1\,\rm GHz}\right)^{-0.12} \times\left(\frac{\Gamma_{\rm jet}-1}{0.06}\right)^{-1}\left(\frac{V}{0.36\,\rm kpc^3}\right)^{-\frac{4}{7}}\ \rm cm^{-3}. \quad (7)$$

[4] Using the Low Frequency Array (LOFAR) between 109 and 183 MHz, at an angular resolution of ∼3.5 arcsec, McKean et al. (2016) found that the low-energy turnover of the secondary hotspots synchrotron spectra in Cygnus A is at ∼150 MHz.

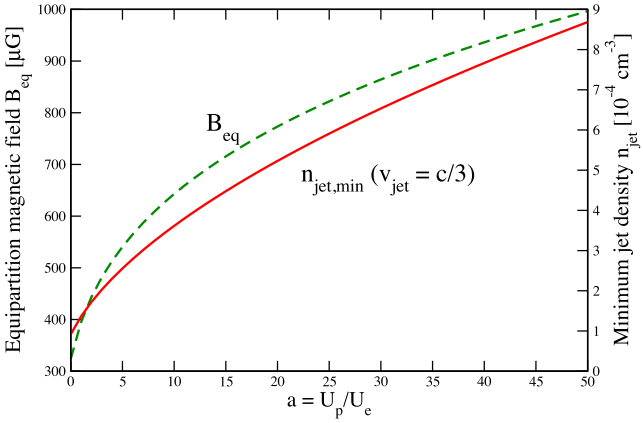

Figure 2. Left-hand axis: magnetic field in equipartition with non-thermal particles: $B_{\rm eq}^2/(8\pi) = (1+a)U_{\rm e}$ (green-dashed line). Right-hand axis: minimum jet matter density ($n_{\rm jet,min}$) considering $v_{\rm jet} = c/3$ (red-solid line).

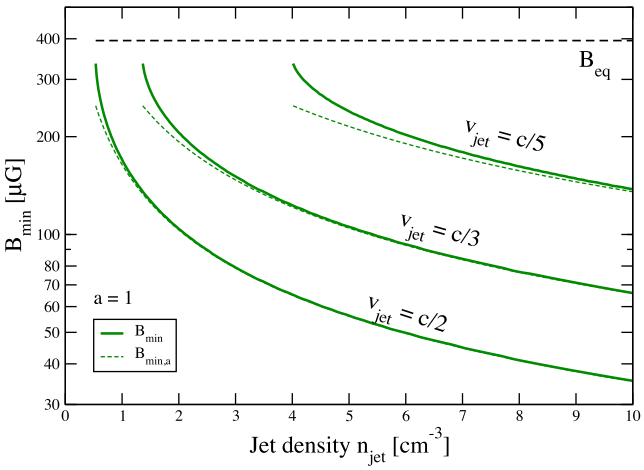

Figure 3. Minimum magnetic field required to explain the flux at 43 GHz. $B_{\rm min}$ (green-solid lines) and $B_{\rm min,a}$ (green-dashed lines) are plotted for the case of $a = 1$ and $v_{\rm jet} = c/2$, $c/3$ and $c/5$. The equipartition magnetic field is also indicated (black-dashed line).

In Fig. 2, we plot $n_{\rm jet,min}$ for $0 \le a \le 50$ and considering $v_{\rm jet} = c/3$. Note that $n_{\rm jet,min} \propto 1/(\Gamma_{\rm jet} - 1)$ and therefore it is ∼3.7 times larger and 0.41 times smaller than the values plotted in Fig. 2 when $v_{\rm jet} = c/5$ and $c/2$, respectively. In Table 1, we list $n_{\rm jet,min}$ for $v_{\rm jet} = c/5$, $c/3$, and $c/2$, and $a = 1$. In relativistic shocks, we do not expect a much larger than 1, and hereafter we consider $a = 1$. Therefore, the energy density in non-thermal particles is $U_{\rm nt} = 2U_{\rm e}$.

Given that $2U_{\rm e} > B^2/(8\pi)$ when $n_{\rm jet} > n_{\rm jet,min}$, most of the jet kinetic energy goes to non-thermal particles when we consider that there is only magnetic and non-thermal energy in the hotspot. Therefore, we find the magnetic field minimum value ($B_{\rm min}$) required to explain the emission at 43 GHz by setting the condition $U_{\rm kin} = 2U_{\rm e} + B_{\rm min}^2/(8\pi)$. In Fig. 3, we plot $B_{\rm min}$ (green-solid line) for $v_{\rm jet} = c/2$, $c/3$, and $c/5$, and from $n_{\rm jet,min}$ to 10^{-3} cm^{-3} ∼ 0.1 $n_{\rm ext}$, where $n_{\rm ext} \sim 10^{-2}$ cm^{-3} is the density in the external medium (e.g. Wilson, Smith & Young 2006). Values of $n_{\rm jet}$ larger than 10^{-3} cm^{-3} would be very unrealistic given that the jet to external medium density ratio in adiabatic flows is expected to be ∼10^{-2}. In fact, Dreher, Carilli & Perley (1987) found that the plasma density in the jet of Cygnus A is smaller than 4×10^{-4} cm^{-3}. In order to provide an analytical expression ($B_{\rm min,a}$) of $B_{\rm min}$, we set the unrealistic condition

$2U_e = U_{kin}$ and therefore

$$\frac{B_{min,a}}{\mu G} \sim 305 \left(\frac{\nu_{min}}{0.1\,GHz}\right)^{-0.15} \times \left[\left(\frac{n_j}{10^{-4}\,cm^{-3}}\right)\left(\frac{V}{0.36\,kpc^3}\right)\left(\frac{\Gamma_{jet}-1}{0.06}\right)\right]^{-\frac{2}{3}}. \quad (8)$$

In Fig. 3, we plot B_{min} and $B_{min,a}$ (green-dashed line), and we see that $B_{min,a}$ is a very good approximation. Finally, the hotspot magnetic field required to explain the synchrotron emission at 43 GHz is $50 \lesssim B \lesssim 400\,\mu G$. We keep V in equations (5) and (8) to show that B_{eq} and $B_{min,a}$, and therefore B_{min}, increases when V is smaller than $0.36\,kpc^3$. This is the case when we take into account that the jet is inclined by an angle $\sim 70^\circ$ with the line of sight (Steenbrugge & Blundell 2008; Boccardi et al. 2016). In such a case, the real extent of the synchrotron emitter is smaller than l_{obs}, and therefore the emitter volume is smaller than $0.36\,kpc^3$ (Meisenheimer et al. 1989).

The hotspot magnetic field could also be constrained by modelling the (synchrotron self-Compton) X-ray emission (see e.g. Wright & Birkinshaw 2004; Stawarz et al. 2007). However, we need to know the X-ray-emitter volume, which is not easy to determine from the data in the X-ray domain.

3 CUT-OFF OF THE SYNCHROTRON SPECTRUM

Diffuse IR (at frequencies 3.798×10^{13} and 6.655×10^{13} Hz) and optical ($\nu_{opt} = 5.45 \times 10^{14}$ Hz) emission was detected with the *Spitzer Space Telescope* and *Hubble Space Telescope*, respectively (Nilsson et al. 1997; Stawarz et al. 2007). The very steep IR-to-optical spectral index, $\alpha_{IR\text{-}opt} \sim 2.16$, indicates that the cut-off of the synchrotron spectrum is $\nu_c < 5 \times 10^{14}$ Hz. Stawarz et al. (2007) suggested that the optical emission is the low-energy tail of the synchrotron self Compton spectrum, as in the case of the Cygnus A north-west secondary hotspot. In such a case, $\nu_c < 5 \times 10^{14}$ Hz. The maximum energy of non-thermal electrons accelerated at the jet reverse shock is $E_{e,max} \sim 0.8$ TeV when $\nu_c = 5 \times 10^{14}$ Hz and $B = 100\,\mu G$, as shown in equation (1).

3.1 Revising the reigning paradigm

It is commonly assumed in the literature that $E_{e,max}$ is determined by synchrotron losses (e.g. Prieto, Brunetti & Mack 2002). In such a case, by equating the synchrotron cooling time, $t_{synchr} \sim 600/(E_{e,max}B^2)$ s, with the acceleration time-scale $t_{acc} \sim 20\mathcal{D}/v_{sh}^2$, where the diffusion coefficient is $\mathcal{D} = \lambda c/3$ and λ is the mean-free path, we find that

$$\frac{\mathcal{D}}{\mathcal{D}_{Bohm}} = \frac{\lambda}{r_g} \sim 2 \times 10^6 \left(\frac{v_{sh}}{c/3}\right)^2 \left(\frac{\nu_c}{5 \times 10^{14}\,Hz}\right)^{-1}. \quad (9)$$

In equation (9) $\mathcal{D}_{Bohm} = r_g c/3$ is the Bohm diffusion coefficient and $r_g = E_{e,max}/(eB)$ is the Larmor radius of $E_{e,max}$-electrons (and protons) in a turbulent field B.

In the small scale turbulence regime $\lambda = r_g^2/s$, where s is the plasma-turbulence scalelength (e.g. Ostrowski & Bednarz 2002; Kirk & Reville 2010; Lemoine & Pelletier 2010; Sironi et al. 2013). Therefore, from equation (9), the plasma-turbulence scalelength in the 'reigning paradigm' is

$$s \sim \frac{r_g^2}{\lambda} = r_g \frac{\mathcal{D}_{Bohm}}{\mathcal{D}} \sim 8.3 \times 10^6 \left(\frac{\nu_c}{5 \times 10^{14}\,Hz}\right)^{\frac{3}{2}} times \left(\frac{B}{100\,\mu G}\right)^{-\frac{3}{2}} \left(\frac{v_{sh}}{c/3}\right)^{-2} cm. \quad (10)$$

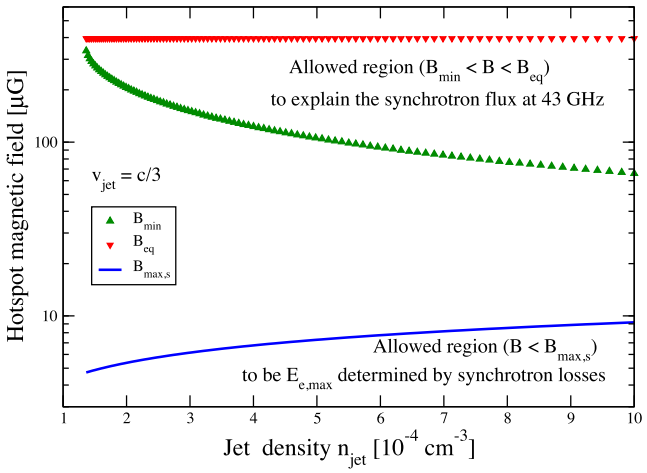

Figure 4. Comparison between the magnetic field required to explain the synchrotron flux at 43 GHz ($B_{min} \leq B \leq B_{eq}$) and the magnetic field required to satisfy the condition $s \leq c/\omega_{pi}$ ($B \leq B_{max,s}$). We can see that $B_{max,s} < B_{min}$ and therefore the condition $B \leq B_{max,s}$ is not satisfied.

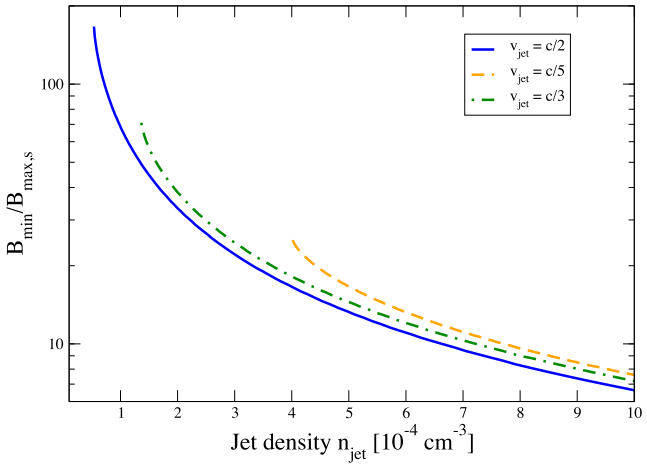

Figure 5. Ratio $B_{min}/B_{max,s}$ for $v_{jet} = c/2$ (blue-solid line), $c/3$ (green-dot–dashed line) and $c/5$ (orange-dashed line).

Surprisingly, s is smaller than the ion-skin depth $c/\omega_{pi} \sim 10^9\,\Gamma_{jet}^{0.5}(n_{jet}/10^{-4}\,cm^{-3})^{-0.5}$ cm unless B is smaller than

$$\frac{B_{max,s}}{\mu G} \sim 2 \left(\frac{\nu_c}{5 \times 10^{14}\,Hz}\right)\left(\frac{n_{jet}}{10^{-4}\,cm^{-3}}\right)^{\frac{1}{3}}\left(\frac{v_{sh}}{c/3}\right)^{-\frac{4}{3}}. \quad (11)$$

(Note that $B_{max,s} \propto \Gamma_{jet}^{-1/3}$, but we neglect this dependence in equation (11) given that $1.02 \leq \Gamma_{jet} \leq 1.15$ when $c/5 \leq v_{jet} \leq c/2$.) In Fig. 4, we plot $B_{max,s}$ (blue-solid line) for the case $v_{jet} = c/3$. We see that B_{min} is larger than $B_{max,s}$ for all possible values of n_{jet}. We mentioned that 5×10^{14} Hz is the upper-limit for the synchrotron spectrum cut-off. In the case that $\nu_c < 5 \times 10^{14}$ Hz, $B_{max,s}$ is even smaller than the value plotted in Fig. 4, whereas B_{min} increases. Therefore, $\nu_c < 5 \times 10^{14}$ Hz enlarges the gap between B_{min} and $B_{max,s}$. Note that $B_{min}/B_{max,s}$ also increases when we consider an emission volume (at 43 GHz) smaller than $0.36\,kpc^3$, as a consequence of the jet inclination angle (e.g. Meisenheimer et al. 1989). In Fig. 5, we plot $B_{min}/B_{max,s}$ for the cases $v_{jet} = c/2$ (blue-solid line), $v_{jet} = c/3$ (green-dot–dashed line) and $c/5$ (orange-dashed line). We can see that $B_{min} > B_{max,s}$ for all possible values of v_{jet} and n_{jet}.

Hence, we show that B is larger than $B_{\rm max,s}$ for a large range of parameters and therefore $E_{\rm e,max}$ cannot be determined by synchrotron cooling in the primary hotspot of Cygnus A, in disagreement with the standard assumption as was pointed out by Araudo et al. (2016). Note that to reach this conclusion, we have only used well-resolved radio emission at 43 GHz and the requirement $s > c/\omega_{\rm pi}$. In the next section, we explore a more fundamental limit to constrain $E_{\rm e,max}$.

4 THE CASE OF PERPENDICULAR SHOCKS

The maximum energy is ultimately constrained by the ability to scatter particles back and forth across the shock, and this depends on the geometry of the magnetic field (i.e. the angle between the field vector and the shock normal). In this section, we consider the case of perpendicular shocks, given that relativistic shocks are characteristically quasi-perpendicular. Note however that shocks moving at $v_{\rm sh} \sim c/3$ are mildly relativistic and therefore they may not be strictly perpendicular. Unfortunately, it is not possible to determine the geometry of the magnetic field in the reverse shock downstream region using the polarization data available in the literature.

4.1 Electrons' maximum energy determined by the diffusion condition

To accelerate particles up to an energy $E_{\rm e,max}$ in perpendicular shocks, the mean-free path in turbulent magnetic field in the shock downstream region, $\lambda_{\rm d} \sim (E_{\rm e,max}/eB)^2/s$ has to be smaller than Larmor radius in $B_{\rm jd}$ in order to avoid the particles following the $B_{\rm jd}$-helical orbits and cross-field diffusion ceasing (Kirk & Reville 2010; Lemoine & Pelletier 2010; Sironi et al. 2013; Reville & Bell 2014). The condition $\lambda_{\rm d} \lesssim r_{\rm g0}$, where $r_{\rm g0} = E_{\rm e,max}/(eB_{\rm jd})$ is the Larmor radius in the ordered (and compressed) field $B_{\rm jd} \sim 4B_{\rm j}$, where $B_{\rm j}$ is the jet magnetic field, is marginally satisfied when the magnetic-turbulence scalelength is $s = s_\perp$, where

$$s_\perp = \frac{E_{\rm e,max}}{eB}\left(\frac{4B_{\rm j}}{B}\right) \sim 6.7\times10^{11}\left(\frac{\nu_{\rm c}}{5\times10^{14}\,{\rm Hz}}\right)^{\frac{1}{2}}\left(\frac{B_{\rm j}}{\mu{\rm G}}\right)\left(\frac{B}{100\,\mu{\rm G}}\right)^{-\frac{5}{2}}{\rm cm}. \quad (12)$$

In Fig. 6, we plot $s_\perp$ for the cases of $B = B_{\rm eq}$ (red-dotted line) and $B = B_{\rm min}$ (green-dotted lines) and fixing $B_{\rm j} = 1\,\mu$G. We also plot $c/\omega_{\rm pi}(\propto n_{\rm jet}^{-0.5})$. Note that $s_\perp > c/\omega_{\rm pi}$, which indicates that the magnetic field is probably not generated by the Weibel instability (that has a characteristic scalelength of $c/\omega_{\rm pi}$).

4.2 NRH instabilities in perpendicular shocks

Turbulence on a scale greater than $c/\omega_{\rm pi}$ may be excited through the NRH instability, which can grow until s reaches the Larmor radius of the highest energy CR driving the instability (Bell 2004, 2005). Since the scattering rate is proportional to E^{-2} in given small-scale turbulence, the distance over which CR currents are anisotropized downstream of the shock is proportional to E^2. Hence, the higher energy CR have more time to drive the NRH instability, and CRs with energy $E_{\rm e,max}$ are predominantly responsible for generating the turbulence, unless the CR spectrum is unusually steep ($p > 3$). As explained above, the maximum CR energy $E_{\rm e,max}$ is that of CR whose anistropy decays over a distance equal to their Larmor radius in the ordered component of the downstream magnetic field (Bell et al. 2017).

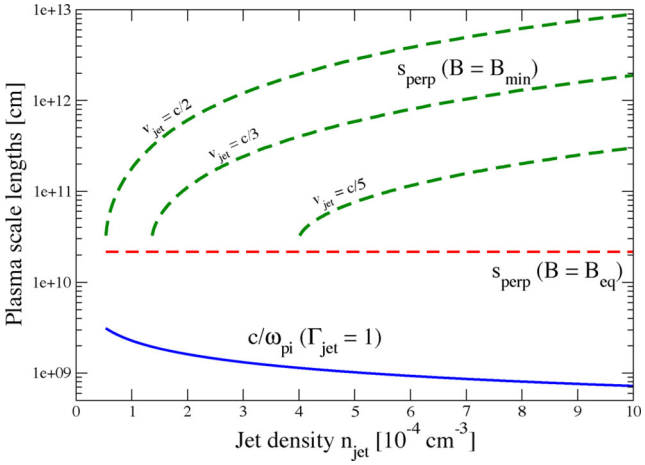

Figure 6. Magnetic turbulence scalelength for the case of perpendicular shocks ($s_\perp$ – dashed lines) and ion-skin-depth $c/\omega_{\rm pi}$ (blue-solid line).

We now discuss whether $E_{\rm e,max}$-CRs have sufficient energy density to amplify the magnetic field. To amplify the magnetic field via the NRH instability in a perpendicular shock, the turbulent field has to grow through around 10 e-foldings at the maximum growth rate $\Gamma_{\rm max}$ (Bell et al. 2013). The time available for the instability to grow is $t_\perp = r_{\rm g0}/v_{\rm d}$, during which the plasma flows through a distance $r_{\rm g0}$ in the downstream region at velocity $v_{\rm d} \sim v_{\rm sh}/4$. Therefore, the condition for magnetic field amplification by the NRH instability in perpendicular shocks is $\Gamma_{\rm max}t_\perp > 10$. In perpendicular shocks where both the CR current $j_{\rm CR}$ and $B_{\rm jd}$ are in the plane of the shock and orthogonal to each other, $\Gamma_{\rm max}$ is similar to the linear growth rate in parallel shocks, as shown by Riquelme & Spitkovsky (2010) and Matthews et al. (2017), and in agreement with the dispersion relation derived by Bell (2005). Therefore, in perpendicular geometry, $\Gamma_{\rm max} \sim (j_{\rm CR}/c)\sqrt{\pi/\rho_{\rm jet}}$, where $\rho_{\rm jet} = m_{\rm p}n_{\rm jet}$.

The current density carried by $E_{\rm e,max}$-CRs is $j_{\rm e,max} = \eta_{\rm e,max}U_{\rm kin}ce/E_{\rm e,max}$, where $\eta_{\rm e,max} = 1$ notionally represents the condition in which the CR electron number density at energy $E_{\rm e,max}$ is equal to $U_{\rm kin}/E_{\rm e,max}$ and the CR drift along the shock surface at velocity c. Allowing for compression of the mass density and magnetic field by a factor of four at the shock, the condition $\Gamma_{\rm max}\,t_\perp > 10$ leads to a lower limit on $\eta_{\rm e,max}$: $\eta_{\rm e,max} > \eta_{\rm min} = 80/M_{\rm A}$ where $M_{\rm A} = v_{\rm sh}/v_{\rm A}$ is the Alfvén Mach number of the jet at the termination shock and $v_{\rm A} = B_{\rm j}/\sqrt{4\pi\rho_{\rm jet}}$, giving

$$M_{\rm A} = 1400\left(\frac{v_{\rm sh}}{c/3}\right)\left(\frac{B_{\rm j}}{\mu{\rm G}}\right)^{-1}\left(\frac{n_{\rm jet}}{10^{-4}\,{\rm cm}^{-3}}\right)^{\frac{1}{2}}, \quad (13)$$

and therefore

$$\eta_{\rm min} = 0.057\left(\frac{v_{\rm sh}}{c/3}\right)^{-1}\left(\frac{B_{\rm j}}{\mu{\rm G}}\right)\left(\frac{n_{\rm jet}}{10^{-4}\,{\rm cm}^{-3}}\right)^{-\frac{1}{2}}. \quad (14)$$

The ordered magnetic field $B_{\rm j}$ in the termination region of AGN jets is unknown, but values lower than 1 μG are reasonable considering the lateral expansion of the jet during propagation from its origin in the active galactic nucleus. It appears that the CR current is sufficient to drive the NRH instability, but the margins are tight, CR acceleration to energy $E_{\rm e,max}$ must be efficient, and the jet magnetic field must be small.

In order to check whether these conditions are satisfied in the primary hotspot of Cygnus A, we consider that non-thermal protons are accelerated in the jet reverse shock following a power-law energy

distribution with the same index as non-thermal electrons ($p = 2.44$). In such a case, the energy density in $E_{\rm e,max}$-protons is $U_{\rm e,max} = K_{\rm p} E_{\rm e,max}^{2-p}$, where $K_{\rm p}$ is the normalization constant of the energy distribution. Considering that $U_{\rm e} = U_{\rm p}$ (see Section 2.1), we find $K_{\rm p} = U_{\rm e}(p-2)/E_{\rm p,min}^{2-p}$ where $E_{\rm p,min}$ is the minimum energy of non-thermal protons. By setting $E_{\rm p,min} = 1$ GeV, we find that the acceleration efficiency of $E_{\rm e,max}$-protons is

$$\eta_{\rm e,max} \equiv \frac{U_{\rm e,max}}{U_{\rm kin}} \sim 0.44 \left(\frac{U_{\rm e}}{U_{\rm kin}}\right)\left(\frac{E_{\rm e,max}}{\rm GeV}\right)^{-0.44}$$
$$\sim 0.07 \left[\left(\frac{\nu_{\rm c}}{5\times10^{14}\,{\rm Hz}}\right)\left(\frac{\nu_{\rm min}}{0.1\,{\rm GHz}}\right)\right]^{-0.22}\left(\frac{B}{100\,\mu{\rm G}}\right)^{-1.28}$$
$$\times \left[\left(\frac{n_{\rm jet}}{10^{-4}\,{\rm cm}^{-3}}\right)\left(\frac{\Gamma_{\rm jet}-1}{0.06}\right)\left(\frac{V}{0.36\,{\rm kpc}^3}\right)\right]^{-1}. \quad (15)$$

Therefore, to satisfy the condition $\eta_{\rm e,max} > \eta_{\rm min}$ (equation 14) for efficient magnetic field amplification by the NRH-instability in a perpendicular shock, the jet (unperturbed) magnetic field has to be

$$\left(\frac{B_{\rm j}}{\mu{\rm G}}\right) < 1.2\left(\frac{n_{\rm jet}}{10^{-4}\,{\rm cm}^{-3}}\right)^{-\frac{1}{2}}\left(\frac{B}{100\,\mu{\rm G}}\right)^{-1.28}\left(\frac{\Gamma_{\rm jet}-1}{0.06}\right)^{-1}, \quad (16)$$

when V, $\nu_{\rm c}$ and $\nu_{\rm min}$ take the values in Table 1, and $\nu_{\rm sh} \sim c/3$. In such a case, and assuming that the shock is quasi-perpendicular, $E_{\rm e,max}$-CRs have sufficient energy density to generate NRH-turbulence on scale $s_\perp$ and amplify the magnetic field by a factor $B/B_{\rm j} \sim 100$ in the primary hotspot of Cygnus A.

5 CONCLUSIONS

We study diffusive shock acceleration and magnetic field amplification in the north-west primary hotspot in Cygnus A. We focus on the well-resolved region downstream of the jet reverse shock where most of the synchrotron radiation is emitted. By considering the synchrotron flux at 43 GHz, we determine that the jet density has to be larger than $\sim 5 \times 10^{-5}\,{\rm cm}^{-3}$ and the hotspot magnetic field is $50 \lesssim B \lesssim 400\,\mu$G (when the energy density in non-thermal protons is the same as in non-thermal electrons, i.e. $a = 1$, and $c/5 < v_{\rm jet} < c/2$). The cut-off of the synchrotron spectrum is at $\nu_{\rm c} \lesssim 5 \times 10^{14}$ Hz, implying that the maximum energy of electrons accelerated in the hotspots is $E_{\rm e,max} < 1$ TeV. By setting the magnetic-turbulence scalelength s larger than the ion-skin depth $c/\omega_{\rm pi}$ (in the small-scale turbulence regime), we find that the magnetic field required to be $E_{\rm e,max}$ determined by synchrotron cooling is smaller than the field required to explain the synchrotron emission at 43 GHz. Therefore, we conclude that $E_{\rm e,max}$ is not constrained by synchrotron cooling, as traditionally assumed.

The maximum energy $E_{\rm e,max}$ is ultimately determined by the scattering process. By assuming that the shock is quasi-perpendicular, particles cannot diffuse further than a distance $r_{\rm g0}$ downstream of the shock, i.e. $\lambda_{\rm d} < r_{\rm g0}$. To satisfy this condition, the magnetic turbulence scalelength has to be larger than $\sim 2 \times 10^{10}$ cm, that is $\sim 10\, c/\omega_{\rm pi}$ (see Fig. 6), and therefore B is probably not amplified by the Weibel turbulence.

On the other hand, the NRH instability amplify the magnetic field on scales larger than $c/\omega_{\rm pi}$ and we show that NRH-modes generated by CRs with energies $E_{\rm e,max}$ can grow fast enough to amplify the jet magnetic field from ~ 1 to 100 μG and accelerate particles up to energies $E_{\rm e,max} \sim 0.8$ TeV observed in the primary hotspot of Cygnus A radiogalaxy. The advantage of magnetic turbulence being generated by CRs current is that B persists over long distances downstream of the shock, and therefore particles accelerated very near the shock can emit synchrotron radiation far downstream.

Finally, if $E_{\rm e,max}$ is determined by the diffusion condition in a perpendicular shock, the same limit applies to protons and therefore the maximum energy of ions is also $\sim$0.8 TeV. As a consequence, relativistic shocks in the termination region of FR II jets are poor cosmic ray accelerators.

ACKNOWLEDGEMENTS

The authors thank the anonymous referee for a constructive report. The authors thank S. Pyrzas for providing Fig. 3 in Pyrzas et al. (2015), and Alexandre Marcowith and Robert Laing for useful comments. The research leading to this article has received funding from the UK Science and Technology Facilities Council under grants ST/K00106X/1 and ST/N000919/1. A.T.A. acknowledges the financial support of the Agence National pour la Recherche through the Labex Ocevu: OCEVU Labex (ANR-11-LABX-0060).

REFERENCES

Araudo A. T., Bell A. R., Crilly A., Blundell K. M., 2016, MNRAS, 460, 3554
Bell A. R., 2004, MNRAS, 353, 550
Bell A. R., 2005, MNRAS, 358, 181
Bell A. R., Schure K. M., Reville B., Giacinti G., 2013, MNRAS, 431, 415
Bell A., Araudo A., Matthews J., Blundell K., 2017, MNRAS, preprint (arXiv: 1709.07793)
Boccardi B., Krichbaum T. P., Bach U., Mertens F., Ros E., Alef W., Zensus J. A., 2016, A&A, 585, A33
Brunetti G., Mack K.-H., Prieto M. A., Varano S., 2003, MNRAS, 345, L40
Carilli C. L., Perley R. A., Dreher J. W., Leahy J. P., 1991, ApJ, 383, 554
Dreher J. W., Carilli C. L., Perley R. A., 1987, ApJ, 316, 611
Hillas A. M., 1984, ARA&A, 22, 425
Kirk J. G., Reville B., 2010, ApJ, 710, L16
Lagage P. O., Cesarsky C. J., 1983, A&A, 125, 249
Leahy J. P., Muxlow T. W. B., Stephens P. W., 1989, MNRAS, 239, 401
Lemoine M., Pelletier G., 2010, MNRAS, 402, 321
Mack K.-H., Prieto M. A., Brunetti G., Orienti M., 2009, MNRAS, 392, 705
Matthews J. H., Bell A. R., Blundell K. M., Araudo A. T., 2017, MNRAS, 469, 1849
McKean J. P. et al., 2016, MNRAS, 463, 3143
Meisenheimer K., Heavens A. F., 1986, Nature, 323, 419
Meisenheimer K., Roser H.-J., Hiltner P. R., Yates M. G., Longair M. S., Chini R., Perley R. A., 1989, A&A, 219, 63
Nilsson K., Valtonen M. J., Jones L. R., Saslaw W. C., Lehto H. J., 1997, A&A, 324, 888
Norman C. A., Melrose D. B., Achterberg A., 1995, ApJ, 454, 60
Orienti M., Brunetti G., Nagai H., Paladino R., Mack K.-H., Prieto M. A., 2017, MNRAS, 469, L123
Ostrowski M., Bednarz J., 2002, A&A, 394, 1141
Owen F. N., Ledlow M. J., Morrison G. E., Hill J. M., 1997, ApJ, 488, L15
Perlman E. S., Georganopoulos M., May E. M., Kazanas D., 2010, ApJ, 708, 1
Prieto M. A., Brunetti G., Mack K.-H., 2002, Science, 298, 193
Pyrzas S., Steenbrugge K. C., Blundell K. M., 2015, A&A, 574, A30
Rachen J. P., Biermann P. L., 1993, A&A, 272, 161
Reville B., Bell A. R., 2014, MNRAS, 439, 2050
Riquelme M. A., Spitkovsky A., 2010, ApJ, 717, 1054

Sironi L., Spitkovsky A., Arons J., 2013, ApJ, 771, 54
Stawarz Ł., Cheung C. C., Harris D. E., Ostrowski M., 2007, ApJ, 662, 213
Steenbrugge K. C., Blundell K. M., 2008, MNRAS, 388, 1457
Tingay S. J., Lenc E., Brunetti G., Bondi M., 2008, AJ, 136, 2473
Wilson A. S., Young A. J., Shopbell P. L., 2000, ApJ, 544, L27
Wilson A. S., Smith D. A., Young A. J., 2006, ApJ, 644, L9
Wright M. C. H., Birkinshaw M., 2004, ApJ, 614, 115

This paper has been typeset from a TEX/LATEX file prepared by the author.